

ULRR

Spherical indentation of free-standing acellular extracellular matrix membranes

Item Type	Article
Authors	Cloonan, Aidan J.;O'Donnell, Michael R.;Lee, William T.;Walsh, Michael T.;De Barra, Eamonn;McGloughlin, Timothy M.
Citation	Acta Biomaterialia;2012 8(1), pp. 262-273
Publisher	Elsevier
Download date	2026-03-06 14:50:02
Item License	https://creativecommons.org/licenses/by-nc-sa/1.0/
Link to Item	https://hdl.handle.net/10344/2132

Spherical Indentation of free-standing acellular Extracellular Matrix Membranes

Aidan J. Cloonan^{a,b}, Michael R. O'Donnell^{a,b}, William T. Lee^c, Michael T. Walsh^{a,b}, Eamonn DeBarra^a,
Tim M. McGloughlin^{a,b*}

^a *Centre for Applied Biomedical Engineering Research (CABER), Department of Mechanical, Aeronautical and Biomedical Engineering, University of Limerick, Limerick, Ireland*

^b *Materials and Surface Science Institute, University of Limerick, Limerick, Ireland*

^c *Mathematics Applications Consortium for Science and Industry (MACSI) Department of Mathematics & Statistics, University of Limerick, Limerick, Ireland*

* Corresponding Author:

Tim McGloughlin

A1096

Centre for Applied Biomedical Engineering Research (CABER)

Materials and Surface Science Institute

Dept. of Mechanical, Aeronautical and Biomedical Engineering,

University of Limerick

Ireland

Tim.McGloughlin@ul.ie

Tel: + 353 (0) 61232217 Fax: +353 61202944.

Author email addresses:

Aidan J. Cloonan: Aidan.Cloonan@ul.ie

Michael R. O'Donnell: Michael.O'Donnell@ul.ie

William T. Lee: William.Lee@ul.ie

Michael T. Walsh: Michael.Walsh@ul.ie

Eamonn DeBarra: Eamonn.DeBarra@ul.ie

Tim M. McGloughlin: Tim.McGloughlin@ul.ie

1 1. Introduction

2 Extracellular matrix materials (ECMs) are bioresorbable, naturally occurring scaffolds that have been used
3 extensively for tissue and organ reconstruction. Of the range of ECM materials developed, porcine-derived small
4 intestinal submucosa (SIS) has been the most investigated and implanted, the most clinically successful example
5 being Biodesign™ Surgisis® (Cook Biotech, West Lafayette, IN, USA), used in more than one million procedures
6 to date. The biomolecular complexity of these scaffolds, retaining a variety of collagen types, glycosaminoglycans,
7 growth factors and adhesion ligands [1-3], distinguishes the host response *in vivo* to that of bioinert and
8 bioresorbable scaffolds. Post-implantation, the ECM is remodelled rather than simply degrading or resorbing. Cells
9 repopulate the scaffold during remodelling from adjacent tissues and additionally blood- and marrow-borne derived
10 cells translocate to the implant site, differentiating into specific phenotypes. Porcine-derived Urinary Bladder Matrix
11 (UBM) cardiac patches have been previously reported to progress towards a collagen-rich vascularised myocardial
12 replacement after 3 months *in vivo* [4]. Long-term recruitment of marrow cells has been observed in a tendon gap
13 animal model for an intact SIS ECM, compared to SIS chemically stripped of bioactive components [5].

14 As ECM materials remodel, the mechanical properties and strength changes over time [6]. Ideally, both scaffold
15 and tissue should have similar compliance and sufficient mechanical properties to prevent failure *in vivo*. However,
16 ECM materials possess inherent variation in mechanical properties. Thickness and mechanical properties vary due to
17 factors such as source variables (animal age [7], diet, breed, etc.), processing (manual versus machine [8]),
18 decellularisation protocol and method of terminal sterilisation [2, 9]. The location of harvest also introduces
19 variation; for example distal SIS was found to be significantly stronger, more elastic and less permeable to urea,
20 compared to proximal SIS [8]. To increase ECM strength and achieve consistent mechanical properties,
21 reinforcement by physical means (e.g. via lamination, stitching, surgical mesh or non-woven layer reinforcement) or
22 chemical cross-linking may be employed. The collagenous microstructure of tissues and derived ECM material often
23 possess a degree of alignment or anisotropy, dependent on the organs' functionality and mechanical stimuli. For
24 example, tendons, ligaments, oesophagus and arterial vessels display distinct anisotropy whereas stomach and
25 cholecyst display more isotropic or weakly anisotropic material properties.

26 As these ECM materials are employed to repair or replace damaged or missing tissues and organs, it is
27 important that the material properties are identified prior to implantation, in order to maximise clinical utility. For

1 biomaterials which are anisotropic and hyperelastic and modelled with a strain energy function, uniaxial tension is
2 insufficient for mechanical characterisation. Evaluation of biaxial strains in hyperelastic membranes can be
3 investigated via in-plane biaxial stretching, axisymmetric inflation or axisymmetric indentation [10-12]. However
4 planar biaxial testing is generally limited by its inability to test specimens to failure [13]. Applying biaxial tension
5 via an efficient specimen gripping protocol is challenging, typically compounded by the soft, deformable nature of
6 biological specimens. Hooks [14], sutures [11, 12, 15], clamps [16], needles and tines [17] have been previously
7 utilised in biaxial setups, but these point forces along the specimen edges can result in non-uniform stress and strain
8 distributions. To alleviate this, a small central portion of the specimen is generally analysed and cruciform shapes
9 have been utilised [18], in accordance with St. Venant's principle. Waldman *et al.* demonstrated that changing from
10 tethering to a clamping method generated substantially different stress strain curves in the same tissue [19], later
11 attributing this to dramatically different strain regions in the vicinity of the clamps using small angle light scattering
12 (SALS) [20]. It is recommended that the majority of the specimen extracellular reinforcing fibers are effectively
13 contained within the grips in order to minimize testing artefacts [18] and this mode of constraint is implemented
14 with the ASTM standard ball-burst test. Similarly, a circular clamp is used in the classical axisymmetric membrane
15 inflation testing, however a more sophisticated experimental system is required [10]. Measurement of burst strength
16 is recommended in the international standard for vascular implants, *Cardiovascular implants – tubular vascular*
17 *prostheses* (ANSI/AAMI/BS/ISO 7198). The ball burst test has been applied to a variety of biological materials,
18 such as abdomen wall [6], dermis [21] and human acellular dermal matrix dermal ECM (D-ECM) [22], ventricle
19 [23], cardiac-ECM (C-ECM) [23], cholecyst (Ch-ECM) [24], small intestinal submucosa (SIS) [6, 25], urinary
20 bladder matrix (UBM) [25, 26], stomach submucosa (SS) [26], urinary tunica propria and submucosa (UBS) [26],
21 ovine forestomach matrix (OFM) [27] and silk fibroin [28], demonstrating the utility of the technique. Unlike micro-
22 and nano-indentation, a free-standing rather than a supported membrane is indented to failure with a spherical
23 geometry to minimise stress concentrations [29]. Traditionally force at failure (ball burst force) and elongation at
24 failure have been reported; however the ball burst test specimen geometry deformation is complex, making
25 calculation of membrane stresses non-trivial.

26 The objective of the present study is to advance the capability of the ASTM standard ball burst test, focusing on
27 the characterisation of multilaminated ECM materials. An optimum rehydration protocol was initially established by
28 quantifying water absorption and monitoring the effects of hydration on ECM mechanical properties in real-time

1 using Dynamic Mechanical Analysis (DMA) and hydration relaxation experiments. Ball burst tests were then carried
2 out on each membrane material. Membranes analysed included model poly(dimethylsiloxane) (PDMS) hyperelastic
3 membranes and two and four layer multilaminated UBM and SIS materials. PDMS is included as a control
4 hyperelastic isotropic material so comparisons can be made to the ECM membranes evaluated. Along with
5 identifying burst strength, this study also analytically derives material coefficients that describe the behaviour of
6 these materials under biaxial loading. The analytical solution of the spherical indentation of free-standing
7 membranes in the finite strain regime, as proposed by Yang and colleagues [30, 31], is developed to define the
8 material coefficients belonging to the Mooney-Rivlin strain energy function. These material coefficients are then
9 employed in a finite element analysis (FEA) of the experimental procedure. The numerical stress and deformation
10 for each material are then compared to the analytically derived stresses to validate the analytical methodology.

1
2

2. Materials and Methods

2.1 Preparation of Silicone Membranes

Thin PDMS membranes were fabricated using a Spin 150 (SPS-Europe B.V., The Netherlands) spin coater. PDMS is a versatile hyperelastic material which has been utilized in a number of biomedical applications, such as cell response to substrate stiffness [32] and aneurysm experimental models [33, 34]. Silicone elastomer was prepared from a two part Sylgard 184 elastomer kit (Dow Corning Corp. Midland, MI). These comprised primarily of a reaction mixture having a vinyl end-capped oligomeric dimethyl siloxane, a methyl hydrosiloxane cross-linking agent and a platinum catalyst for the hydrosilation reaction. Part A and B contained 30–60 and 10–30 wt%, respectively, of dimethylvinylated and trimethylated silica fillers, as reported by the manufacturer. Both components were added at the recommended 10:1 base-catalyst ratio by mass and stirred in a plastic cup using a glass rod. Trapped air bubbles were removed by degassing under vacuum and solution added drop-wise onto a clean 3" silicon wafer to prevent bubbles. The total spin time was 60 seconds at an acceleration of 20 rpm/s and spin rate of 500 rpm to create a thin, uniform membrane. The PDMS membranes were then cured in an oven at 50°C for 8 hours.

2.5 Preparation of Extracellular Matrix Material

Preparation of acellular UBM and SIS has been previously described [6, 35] and a brief synopsis is outlined. UBM sheets were prepared from porcine bladders; the muscularis externa, submucosal layers and connective tissue were removed leaving the tunica propria and underlying basement membrane. SIS sheets were prepared from porcine small intestine; in brief, the tunica muscularis externa and the majority of the tunica mucosa were removed. SIS material composed of the remaining tunica submucosa, muscularis mucosa and basilar portion of the tunica mucosa. Decellularisation and disinfection was carried out by immersion in 0.1% (v/v) peracetic acid, 4% (v/v) ethanol and 96% (v/v) deionised water for 2 h. The ECM material was then washed twice for 15 min with phosphate buffered saline (pH = 7.4) and twice for 15 min with deionised water. Multi-layered laminated sheets were manufactured by vacuum pressing, lyophilised and terminally sterilized with ethylene oxide (EtO) prior to use. The UBM scaffolds were layed up with luminal surfaces facing outwards and SIS sheets were oriented in parallel. Two and four layer materials were evaluated in this study.

1
2 *2.3 Scanning Electron Microscopy and Surface Topography Analysis*

3 Specimens were cut from the membrane materials and mounted flat with adhesive carbon tabs onto stubs. As the
4 ECM materials were lyophilised, dehydration and fixation was unnecessary. Mounted specimens were sputter-
5 coated (Emitech K550) with a conductive layer of gold under vacuum and imaged at an accelerating voltage of 5 kV
6 using a Hitachi SU-70 high resolution field emission scanning electron microscope (SEM). A series of images tilted
7 between 0 – 30° were captured for each specimen using a motorised eucentric stage and the key 3D reconstruction
8 parameters (working distance, pixel size and tilt angle) were recorded. Stereopair SEM images were processed with
9 the image analysis software program MeX v5.1 (Alicona Imaging GmbH, Graz, Austria). Calibration was initially
10 carried out using a surface roughness specimen (Type 112 1107) having a Ra value of 5.8 µm. Roughness
11 measurements conforming to ISO 4287 were averaged from 5 line profiles per stereopair. Four stereopairs were
12 analysed per specimen.

13 *2.4 Thickness Measurements*

14 Thicknesses were manually recorded as an average of ten measurements along the cross-section of each
15 membrane at a constant force of 5 N using a digital micrometer (MDC-25P, Mitutoyo, Tokyo, Japan) with a
16 resolution of 0.001 mm. The mean dry thicknesses were then used for determining nominal stress values and are
17 identified in Table 1.

18 *2.5 Water Absorption Measurements*

19 Disks were punched (diameter = 5.5 mm) from randomly selected multilaminated ECM sheets. Each dry
20 specimen was weighed to an accuracy of ±0.0001 g (Model AP250D Analytical Plus Balance, Ohaus) and immersed
21 in a thermostatically controlled incubator at 37 ± 0.2°C for durations of 5, 10, 15 and 60 minutes. They were then
22 blotted twice with a lint free cloth to remove surface water and re-weighed. Water absorption was calculated,
23 expressed as increase in weight percent. A minimum of four specimens were evaluated per membrane material.

24 *2.6 Hydration Relaxation*

25 Hydration relaxation testing was performed on single and quadruple ply ECM material to establish baseline
26 hydration durations. Lyophilised ECM sheets (60 x 25 mm) were uniaxially tensioned to 10 N in a custom mini-
27 tensile test stand equipped with a 50 N BFG force gauge (Mecmesin Ltd, UK). After an initial stabilisation period,

1 the dry ECM materials were then continuously hydrated at 37°C and force readings recorded at 10 Hz until no
2 significant change was noted.

3 2.7 *Dynamic Mechanical Analysis (DMA)*

4 DMA testing was carried out in tension mode on a Tritec TTDMA (Triton Technology, UK), equipped with a
5 10 N load cell with a resolution of ± 0.002 N and an immersion bath accessory. Lyophilised ECM sheets were cut
6 into 12 x 5.6 mm specimens and mounted in a thin film clamp with a gauge length of 10 mm and hydrated for 30
7 seconds. Testing was subsequently carried out at several incremental frequencies with a dynamic strain of 0.2%,
8 immersed at 37°C, until no further material response was recorded. DMA utilises a sinusoidal loading (stress)
9 applied to the specimen and the material response (strain) is measured with a Linear Variable Differential
10 Transformer (LVDT). The real or in-phase storage modulus (E') represents the amount of elastic stored energy and
11 can be considered equivalent to a stiffness measurement. The imaginary or out-of-phase loss modulus (E'')
12 represents the viscous behaviour of the material and its ability to recover from deformation. Cycles of increasing
13 frequency were applied to the specimens, ranging from 0.1 to 45 Hz. This frequency range covers typical timescales
14 of periodic scaffold loading *in vivo* [36] (e.g. peristalsis, skeletal movement, blood flow). The highest frequencies
15 are relevant to the ECM viscoelastic response to fast loading events and to evaluate the durability of the inter-ply
16 bonding. Relevant guidance standards are ASTM D4065 and ISO 6721. Isochronal testing was also performed at 1
17 Hz to identify potential longer-term hydration effects on ECM viscoelastic properties. Specimens were evaluated in
18 triplicate.

19 2.8 *Ball Burst Testing*

20 The ball burst test fixture was designed per current ball burst test standards (ASTM D6797, D3797 and D3787)
21 which specify a ring clamp with a 44.45mm diameter opening. The inner clamp edges were chamfered to remove
22 potential stress concentrations and P240 sandpaper lined both surfaces to prevent slippage. A shaft was press-fitted
23 into the spark-eroded cavity of a polished, hardened steel ball (diameter = 25.4 mm, surface tolerance of ± 0.005
24 mm) and connected to a 1000 N loadcell. A constant extension rate of 25.4 mm/min was provided by the crosshead
25 of a H25KS test frame (Tinius Olsen, Surrey, UK). Force and displacement of the steel ball was recorded and
26 analysed using QMAT software. Test specimens were hydrated for 10 minutes and wrinkle-free membranes were

1 tested immediately. A minimum of four specimens were evaluated per membrane material. The burst force was
2 recorded in Newtons (N) and the displacement in millimetres (mm).

3 *2.8 Finite Element Modeling*

4 Finite element simulation of the spherical indentation of free-standing membranes was performed in the finite
5 element software MSC.MARC 2010 (MSC Software Corporation, CA, USA). A hemispherical ball was modelled as
6 a rigid body with a vertical displacement boundary condition applied mimicking the recorded experimental
7 displacement. The circular membranes were modelled using four node Type75 shell elements. Two rigid surfaces
8 representing the experimental clamps constrained the membrane while the rigid ball indenter deformed the
9 hyperelastic membrane. Zero friction was assumed between the smooth indenter and membrane as the ECM
10 multilaminates were hydrated during testing and based on previous experimental reports [37, 38]. A 'glue' contact
11 condition was defined between the two rigid clamps and membrane. The Mooney-Rivlin strain energy density
12 function was employed as the material model. The material coefficients of this material model were identified from
13 the experimental measurements and are identified in Table 1. Computational stresses in the circumferential and
14 radial directions were then resolved and compared to the analytically derived stresses of the same principal
15 directions.

16 *2.10 Statistical Analysis*

17 A one-way analysis of variance was used to determine any differences between groups with a Tukey's post hoc
18 test used to determine differences between pairs. A P value of less than 0.05 was considered significant. All
19 statistical analysis used PASW Statistics v18 Software (SPSS, IBM, Chicago, IL, USA). Values are presented as
20 mean \pm standard deviation.

21 **3. Results**

22 *3.1 Thickness measurements*

23 The average dry sample thickness was calculated as $133 \pm 0.01 \mu\text{m}$ for PDMS. Increasing the amount of ECM
24 layers from 2- to 4- layers caused a significant increase in thickness ($p < 0.05$). UBM thickness increased from 209
25 $\pm 19\mu\text{m}$ to $280 \pm 12 \mu\text{m}$. Similarly, SIS thickness increased from $185 \pm 16\mu\text{m}$ to $205 \pm 21\mu\text{m}$. Lyophilisation
26 significantly decreases ECM thickness, typically by 30% [2], as water and glycosaminoglycans (GAGs) are
27 removed. The vacuum pressing process also reduces the thickness of the multilaminate ECM.

1 3.2 Surface Characteristics

2 The specimens were visually inspected and examined at high magnification using SEM to investigate surface
3 uniformity and quality, see Fig.1. The PDMS membranes exhibited extremely smooth, uniform surface
4 characteristics. No air bubbles, particulate or pinhole defects were observed in the PDMS membranes at high
5 magnification, which could act as sources of localised weaknesses [34]. In the case of the multilaminate ECMs,
6 voids and cracks could potentially cause premature device failure. Qualitatively, UBM displayed a visibly smoother
7 surface than SIS consistent with an intact basement membrane, undisrupted after the lamination process. The SIS
8 surface topography was similar in roughness and porosity to the connective tissue of the tunica propria forming the
9 abluminal UBM surface. This bimodal architecture is characteristic of UBM – a basement membrane luminal
10 surface functioning as a support and selective barrier and a fibrillar, porous abluminal surface providing structural
11 support and allowing cell penetration and movement. SEM stereopairs were digitally processed to reconstruct the
12 membrane surface topographical features in 3D and quantify surface characteristics. The measured Ra value of the
13 standard was accurate to within 5 nm, representing less than 0.1% difference for sequential profile measurements
14 and demonstrating repeatability. The evaluated membrane roughness parameters are presented in Table 1. SIS
15 multilaminate materials consistently displayed higher Ra and Rq values compared to UBM, representing the mean
16 and standard deviation roughness, respectively. Increasing the number of ECM plies from 2 to 4 resulted in higher
17 roughness mean peak to valley height (Rz) values, indicating that additional layering resulted in more variable
18 surface topography characteristics. 3D digital elevation models and anaglyph images are available in the
19 supplementary data.

20 3.3 Effects of ECM Rehydration

21 On average the weight of the SIS devices increased by ~200% after 60 minutes immersion at 37 °C, compared
22 to ~130% for the UBM devices (Fig.2). Generally there was a large variation in water absorbed after 5 minutes,
23 more prominent in the thicker multilaminate materials. Structural damage during processing and material
24 inhomogeneities likely results in hysteresis at short rehydration durations, similar to previous reports [25]. A loss of
25 rehydration ability is likely due to GAG removal and has been previously documented as ~ 60% of the original wet
26 weight [6]. After 60 minutes all ECM materials were characterised by a tighter distribution of water absorption,
27 implying that they had further stabilised. Results from the hydration relaxation experiment are presented in the form
28 of force measurements rather than stress due to the varying levels of compression of the ECM devices (Fig.3a).

1 Single layer ECM material was observed to rehydrate within the initial 10 - 15 seconds, whereas the rehydration rate
2 of the thicker, more compressed ECM multilaminates trended towards 100 - 120 seconds (Fig.3a). Single layer
3 ECM material was observed to rapidly rehydrate within 10 - 15 seconds (data not shown). DMA multi-frequency
4 analysis revealed that SIS consistently displayed a significantly stiffer response compared to UBM (Fig.3a). The
5 ECM bond interfaces remained intact up to ~ 16 Hz, beyond this frequency there was a sharp decrease in E'' with a
6 corresponding increase in the viscous loss modulus, indicating a loss in structural integrity for both 2 ply UBM and
7 SIS membranes. DMA evaluation at 1 Hz for 30 minutes revealed that both moduli stabilised after the initial 5
8 minutes of immersion with no significant transitions for the test duration (data not shown).

9 *3.4 Ball Burst Testing*

10 Ball Burst failure forces for ECM devices evaluated in the current study are compared to a range of ECM
11 materials and source tissues extracted from literature, illustrated in Fig. 4. The ball burst force-indentation curves
12 exhibited initial toe regions followed by a more linear region at higher strain, characteristic of hyperelastic materials
13 and soft tissues, see Fig.5. ECM materials displayed sub-failure arrests, more pronounced in the 4 layer material.
14 This can be attributed to incremental failure of layers within the laminate. Upon failure the ball penetrated through
15 all membrane materials. PDMS membranes displayed a high elongation of 27.85 ± 2.76 mm and a ball burst force of
16 39.26 ± 6.75 N at failure. In contrast the ECM materials displayed stiffer behaviour under loading. Lamination
17 significantly increased the ball burst strength of all ECM devices ($p < 0.01$). Additional layering strengthened the
18 UBM devices by 96%, increasing the ball burst force from 85.96 ± 29.41 N to 168.20 ± 12.24 N ($p < 0.05$).
19 Similarly, increasing from 2 to 4 layer SIS multilaminates resulted in an 81% ball burst force increase from $73.67 \pm$
20 7.66 N to 133.53 ± 21.31 N, respectively ($p < 0.01$). Elongation at failure was not significantly affected by additional
21 layering of the ECM devices.

22 *3.5 Analytical Model of Membrane Deformation*

23 Analytical force-deflection model fits were derived from the experimental measurements, based on the
24 theoretical methodology outlined in Appendix A. The analytical force-deflection models accurately described the
25 biaxial behaviour of all materials tested in this study (Fig.5). The model slightly underestimated PDMS indentation
26 forces at small deflections, but displayed a better fit to the ECM force - deflection data. The material coefficients
27 employed for these analytical force-deflection curves were derived and are tabulated in Table 1. The magnitude of

1 the material coefficients are similar for all ECM materials tested in this study. The material coefficients for PDMS
2 are significantly smaller than the ECM materials evaluated, as PDMS is a much more compliant hyperelastic
3 material.

4 3.6 Comparison of computational and analytical solutions

5 The maximum deflections for both analytical and FE solutions display good correlation, as illustrated in Fig.6.
6 This is expected in the contact region between the membrane and the spherical indenter; however, for all materials
7 evaluated, the deformation profiles in the non-contact region also display good agreement. Circumferential stress
8 resultants calculated from the FE simulations compared well with the analytically-derived circumferential stress
9 resultants. Circumferential stress resultant - strain curves of the evaluated materials are presented in Fig.7. The
10 reduced cross-sectional area of the thinner ECM laminates resulted in higher stresses at equivalent strains, compared
11 to the thicker and more compressed 4 ply devices.

12 4. Discussion

13 When designing an implantable ECM scaffold one must consider initial hydration, biaxial loading conditions *in*
14 *vivo* and a strength decrease due to scaffold degradation within 60 – 90 days [39]. The ECM scaffold must have
15 sufficient mechanical properties to maintain the repair initially, shifting to a reinforcement role with subsequent
16 remodelling, tissue ingrowth and maturation over time. This is illustrated by increased ball burst strength for
17 explanted SIS, compared to the original implant, see Fig.4. Constructive ECM remodelling requires early
18 mechanical loading to site-specific physiological levels; such as bladder filling in a partial cystectomy model [40]
19 and unrestricted motion in an Achilles tendon model [41]. Without loading, ECM constricts and often forms
20 granulation tissue [40].

21 Generally lyophilised ECMs are aseptically rehydrated prior to clinical use, *in vitro* cell culture and mechanical
22 characterisation. There is a paucity of published studies on optimum rehydration protocols for lyophilised ECM
23 material. Four layer SIS device stiffness was previously investigated at incremental hydration time points with ball
24 burst testing, recommending a minimum duration of 5 minutes [25], however the ECM processing route and
25 rehydration temperature was not specified. Testing was carried out in the current study in a hydrated state at 37 °C,
26 as recommended by ASTM guidelines, *Standard guide for characterization and testing of biomaterial scaffolds used in*
27 *tissue engineered medical products* (ASTM F2150-07). Insufficient rehydration results in a stiffer material response with

1 higher stresses recorded during uniaxial and biaxial testing. Commercially available examples such as Biodesign®
2 Surgisis™ and Restore® recommend a minimum of 5 minutes and 7-10 minutes rehydration, respectively while 10-
3 40 minutes is recommended for Alloderm®. Some ECM devices, such as XenMatrix™ Surgical Graft and
4 MesoBiomatrix™ are provided hydrated. Lower inflammatory responses have been previously observed for
5 hydrated human acellular dermal matrices (stored in a 70% ethanol solution) when compared to lyophilised grafts
6 (both types hydrated before placement) for hernia repair [22]. Previous work has demonstrated no significant change
7 in ultimate tensile strength and elongation for multilaminate UBM and SIS post 8 weeks hydration [42], however a
8 disadvantage of hydrated storage is leaching of soluble growth factors from the material [2]. The variance in water
9 absorption and rehydration rates of the evaluated ECM devices likely reflects the processing route (dehydration, loss
10 of GAGs and compaction during lyophilisation and vacuum pressing) and source tissue heterogeneity and function.
11 UBM is a thicker ECM derived from bladder tissue, functioning to store and prevent urine passage through the
12 basement membrane whereas SIS is thinner, engaging in gastrointestinal peristalsis and the digestion and absorption
13 of nutrients. We have previously found that decellularised ECM surface characteristics influence initial wettability
14 through dynamic water contact angle measurements, finding that in order of most hydrophobic: abluminal SIS >
15 abluminal UBM > luminal SIS > luminal UBM [43]. To further investigate ECM multilaminate surface
16 characteristics, 3D reconstructions of 2D SEM images were used to quantify topographical features. The advantage
17 of SEM over alternative non-contact techniques such as LCSM and μ -CT is that a maximum resolution of 1 nm can
18 be achieved. Mex employs image reconstruction algorithms to calculate image depth based on the disparity between
19 stereopair images with identical working distances and point sizes, hence accurate tilt angles, contrast and brightness
20 are essential for topography measurements. Quantification of surface topography can be used to regulate properties
21 *in vivo* (e.g. cell attachment and surface thrombogenicity) or to optimise multilaminate construction, as it is likely
22 that increased ECM roughness would increase inter-laminar bond strengths. Higher levels of ECM material
23 dehydration and associated compression during processing also result in increased inter-laminar bonding. It has been
24 previously shown that use of a solvent, constricted cross-linked multi-ply submucosa based scaffolds, conferring
25 increased lamination strength and stiffness properties [44]. Both 2 ply UBM and SIS remained intact up to ~ 16 Hz,
26 revealing the strength of the inter-laminar bonds, without chemical or physical reinforcement .

27 Hydration relaxation and dynamic mechanical analysis were employed in the current study, in a physiological
28 environment hydrated at 37°C. Dry thicknesses were utilised to minimise variation due to rehydration and be more

1 representative of the stress in the fibrous component. Lamination of the ECM material significantly increased
2 relaxation time and water absorption, post rehydration. This can be explained as due to the relative density and
3 increasing from a single bond interface to three, as in the case of the 4 ply material, further increases the ECM
4 construct variability and equilibration times. Both storage and loss moduli displayed initial decreases, correlating to
5 the gradual increase of elasticity and recovery of handling properties within the initial 5 minutes of rehydration (data
6 not shown). The presence of water acts as a plasticiser and reconstitutes the hydrogen bonds of collagenous
7 structures damaged during lyophilisation. At elevated temperature, there is a decrease in E' (data not shown)
8 indicating that the specimens become less stiff and more pliable at physiological and elevated temperatures (normal
9 porcine body temperature is generally 2°C higher than human [45]) due to slippage and stretching of the collagen
10 molecules and fibrils. At very high temperatures the ordered collagen crystalline structure becomes denatured to a
11 random, gelatinous form with greatly reduced stiffness. A minimum rehydration period of 5 minutes at 37°C would
12 hence seem appropriate for the ECM multilaminates evaluated in this study. Increasing the device thickness or
13 chemically cross-linking the ECM increases the minimum hydration duration required.

14 ECM devices are commonly laminated for strength and tailored for isotropic properties [35, 46]. Restore®
15 (DePuy Orthopaedics, Warsaw, IN), is a 10 layer SIS multilaminate configured with 2 layers aligned every 72° [47].
16 SIS is predominantly longitudinally aligned, with occasional collagen fiber populations oriented at approximately ±
17 30° [48]. Cholecyst ECM, possesses a preferred fiber orientation offset by approximately 65° from neck to the
18 fundus axis [24]. Bladders have been shown to exhibit weak anisotropy during filling, with average peak stretch
19 values of ~2.3 and ~1.9 in the longitudinal and circumferential directions, respectively [49]. UBM displays slight
20 preference towards an angle approximately 15° from the neck to the apex axis, sensitive to processing i.e. scraping
21 across versus parallel to the preferred direction [13]. In the current study, lamination significantly increased ultimate
22 ball burst forces for both UBM and SIS materials. Sub-failure arrests corresponding to failure of individual layers
23 and inter-laminate air voids were occasionally noted between the ECM layers during testing. Structure delamination
24 *in vivo*, with subsequent fluid retention and seroma formation is a potential failure mode and has been previously

1 observed using Surgisis for hernia repair in a primate model [50]; this may be prevented with stitching
2 reinforcement. Lamination reinforcement is desirable as chemical cross-linking has been shown to alter scaffold
3 porosity and microstructure, potentially inhibiting cell infiltration and leading to chronic inflammation [51], ectopic
4 mineralisation [52, 53], host versus graft type reaction [54], encapsulation[54, 55] *in vivo*. Non cross-linked ECM
5 scaffolds are indicated for contaminated abdominal wounds because of the antibacterial effects associated with their
6 degradation [56]. Interestingly, it has been previously reported that stomach submucosa displayed decreased ball-
7 burst forces when increased from 2 to 4-ply [35]. The UTS of multilayered ICL constructs was observed to initially
8 increase from 2 to 4 plies (0.6 MPa to 3.1 MPa) and subsequently decrease to 2 MPa with further lamination to 6
9 plies [57]. Beyond this optimum threshold number of plies, ball-burst force (and UTS) will decrease with increased
10 number of plies. To rationalise this, it is hypothesised that as biological materials possess an inherent distribution of
11 strength, an optimum laminate configuration exists for each ECM. Beyond this optimum threshold number of plies,
12 ball-burst forces (and UTS) will decrease with increased number of plies. Peak inter-laminate shear stresses cause
13 failure of the single weakest ply, with subsequent failure of the multilaminate.

14 Intrinsic mechanical properties of ECM materials are often initially identified with uniaxial tensile testing. A
15 recent study demonstrated that uniaxial strip or ringlet testing overestimates actual burst pressure by just over 50%
16 for autologous tissue engineered blood vessels (TEBVs) and 20% for the native tissue [58], thus highlighting
17 inadequacy for biological device lot release tests. This likely reflects material inhomogeneities and the well-known
18 effect where smaller sized specimens display higher strength and lower probability of failure. Additionally, uniaxial
19 tension allows unrestrained fibrous reorientation in the stretch direction. Previous work has demonstrated no
20 significant differences between equibiaxial testing of cholecyst ECM in the principal and perpendicular directions
21 and idealized ball burst stress–strain data [24]. Freytes *et al.* [26] originally proposed a simple analytical
22 methodology to determine the intrinsic mechanical properties of ECM membranes from the ball burst test, but
23 employed uniaxial rather than biaxial tensile testing to determine the constitutive material models. Although the
24 analytical approximation accurately predicted material stretch, significant differences were found between the
25 analytical and FE resolved stress distributions. The maximum tangential modulus is commonly utilised as a measure
26 of stiffness which can be useful in clinical applications, however as these materials are highly non-linear, it is
27 inaccurate to employ the linear modulus as a constitutive material behavior descriptor.

1 The present study successfully employed an analytical solution to identify intrinsic mechanical properties of
2 tissue engineered membranes and determined the material coefficients of the Mooney-Rivlin strain energy function.
3 Unlike the previously proposed ball burst model [26] which assumes uniform stress distributions across the
4 deformed membrane, non-uniform stress distributions were determined analytically and compared favorably to the
5 numerically resolved stress distributions. This validates the methodology and boundary value problem employed
6 here and demonstrates its suitability to analytically describe the deformation profiles and wall stress resultants in a
7 free-standing circular membrane subject to a spherical indentation. As this approach employed membrane theory,
8 deformed wall thickness is not considered in the equations resolving stress resultants; however wall thickness does
9 affect the analytically resolved forces and subsequent stress resultant calculations. This is apparent in Fig. 7, where
10 the 2 ply materials display higher stresses at equivalent strains compared to the thicker laminates. The difference
11 between burst forces and stresses may be accounted for by considering the relative thicknesses and densities of the 4
12 ply materials subject to increased compression. Prior to rupture of the 2 ply laminate, both 2 ply and 4 ply require
13 similar forces to deflect to similar indentations. Further analysis is required to determine the degree to which the
14 wall thickness influences the analytical solution employed in this study.

15 A limitation of this study is that hyperelastic materials such as PDMS and biological materials commonly
16 display hysteresis when loaded and ideally should be preconditioned to the same loading regime in which they will
17 be in service in order to obtain repeatable results. A fixed indentation rate and no mechanical preconditioning was
18 employed in this study, as per the governing standard, hence capturing the first time straining of the material until
19 ultimate failure. A previous study demonstrated negligible hysteresis effects during the indentation of rubber
20 membranes [37], however it is possible that preconditioning could improve the analytical model fit to the PDMS
21 membrane behaviour at small deflections. The proposed methodology may be readily implemented with smaller
22 diameter ball burst geometries and alternative strain energy functions to characterize biomaterial membranes under
23 biaxial loading to failure. However, the main limitation with this test method is that material anisotropy cannot be
24 resolved, hence to fully characterize membrane biomaterials, a combined methodology of planar biaxial tension
25 testing coupled with ball burst test data to failure would be beneficial in identifying material coefficients of a
26 suitable constitutive material model. FE and phenomenological structural models [59] considering ECM fiber
27 population kinematics may then be employed to utilise this combined test approach to generate optimum ECM ply
28 orientations, aspect ratios [60], bonding and lay-ups for tissue repair.

1
2
3
4
5
6
7
8
9
10
11
12
13
14
15
16
17
18
19
20
21
22
23

5. Conclusions

A variety of xenogeneic and autogenic ECM scaffolds and cell based therapies are increasingly being developed for clinical use. This study represents the first comprehensive evaluation of the effects of hydration on lyophilised multilayered ECM mechanical properties. The biaxial ball-burst coupled with a planar biaxial test offers a promising approach for predicting macroscopic material behavior under complex physiological loading conditions for scaffold biomaterials. The analytically predicted stress resultants and indentations display good correlation with numerical models, for both multilaminate ECMs and a model hyperelastic membrane with high elongation properties. DMA is a powerful characterisation tool suitable for rehydration and storage studies, conditioning scaffolds and dynamic or step-wise fatigue testing. A minimum rehydration period of 5 minutes at 37°C is recommended for the multilaminate ECM materials evaluated. This methodology may also potentially be applied to a range of biologic scaffolds for applications such as source tissue evaluation, optimisation of ECM processing protocols and lot release tests.

Acknowledgements

The authors wish to acknowledge our funding sources (i) Irish Research Council for Science, Engineering and Technology (IRCSET), (ii) Enterprise Ireland (EI) and (iii) Mathematics Applications Consortium for Science and Industry, funded by the Science Foundation Ireland Mathematics Initiative Grant 06/MI/005. The authors are grateful for support from Prof. Jay D. Humphrey and Prof. Stephen F. Badylak and DMA technical assistance from Dr. Glynn Van-de-Velde.

Supplementary Information

Figures with essential colour discrimination. Certain figures in this article, particularly Fig. 6, are difficult to interpret in black and white. The full colour images can be found in the on-line version, at doi:

1

2 **APPENDIX A**

3 The general solution to the spherical indentation of an elastic circular membrane was first proposed by Yang
 4 and Hsu in 1971 [31], advancing initial work carried out by Yang and Feng [30], who reduced the system of
 5 equations governing deformations of membranes of revolution, originally formulated via axisymmetric deformation
 6 simplifications [61]. The reduction of these differential equations, from eight to three, facilitates a numerical
 7 solution for the deformation of membranes and led to further analyses dealing with the inflation or indentation of a
 8 membrane. The solution provided by Yang and Hsu [31] is discussed further here, where the membrane, which has
 9 an undeformed radius a , is fixed along its periphery with, or without, a pre-stretch; see schematic in Fig.A.1. A rigid
 10 smooth sphere of radius R is then brought into contact with the membrane at its centre. By further indentation of the
 11 sphere, the membrane is deformed into an axisymmetric surface with the centre area in contact with the sphere. The
 12 plane polar coordinate, r , is employed to describe the position of every point on the undeformed membrane. A point
 13 P' of the deformed membrane is described by two coordinates: ρ , the horizontal distance from P' to the axis of
 14 symmetry and ξ , the meridian arc length between the centre of the membrane and P' . An infinitesimal radial line PQ
 15 on the undeformed membrane is deformed into a meridian arc $P'Q'$ on the deformed surface. In order to solve the
 16 deformation, it is important to identify the following relationships:

$$\xi = \xi(r) \quad (\text{A.1a})$$

$$\rho = \rho(r) \quad (\text{A.1b})$$

17 The material model employed in this solution is the Mooney-Rivlin strain energy function, as defined by Eq. (A.2).
 18 However, the method of solution applies readily to any general isotropic incompressible and hyperelastic material.

$$W = W(I_1, I_2) = C_{10}(I_1 - 3) + C_{01}(I_2 - 3) \quad (\text{A.2})$$

19 where I_1 and I_2 are the first and second strain invariants of the right Cauchy deformation tensor, defined by Eq. (A.3)

$$I_1 = \lambda_1^2 + \lambda_2^2 + \lambda_3^2 \quad (\text{A.3a})$$

$$I_2 = \lambda_1^2 \lambda_2^2 + \lambda_2^2 \lambda_3^2 + \lambda_3^2 \lambda_1^2 \quad (\text{A.3b})$$

1 The principal stretch ratios for the deformed membrane are defined by Eq. (A.4)

$$\lambda_1 = \frac{d\xi}{dr} \quad (\text{A.4a})$$

$$\lambda_2 = \frac{d\rho}{dr} \quad (\text{A.4b})$$

$$\lambda_3 = \frac{1}{\lambda_1 \lambda_2} \quad (\text{A.4c})$$

2 The subscripts 1, 2, and 3 are employed for the corresponding directions for the rest of this paper. Since there is no
 3 external load in the noncontact region, the equations of equilibrium in the meridian and normal directions are
 4 homogenous and are defined by Eq. (A.5)

$$\frac{dT_1}{d\rho} + \frac{1}{\rho}(T_1 - T_2) = 0 \quad (\text{A.5a})$$

$$K_1 T_1 + K_2 T_2 = 0 \quad (\text{A.5b})$$

5 where T_1 and T_2 are the stress resultants per unit edge length in the circumferential and meridian directions,
 6 respectively; K_1 and K_2 are the principal curvatures of the arcs in the corresponding directions which can be
 7 expressed by

$$K_1 = -\frac{\lambda_1 \rho'' - \rho' \lambda_1'}{\lambda_2^2 \sqrt{\lambda_1^2 - \rho'^2}} \quad (\text{A.6a})$$

$$K_2 = \frac{\sqrt{\lambda_1^2 - \rho'^2}}{\rho \lambda_1} \quad (\text{A.6b})$$

1 where the prime denotes differentiation with respect to r and double prime denotes the second differential with
 2 respect to r . From the strain energy function described by Eq. (A.3), a stress-resultant stretch ratio relation for the
 3 membrane can be derived and defined by Eq. (A.7)

$$T_1 = \frac{1}{\lambda_2} \frac{\partial W}{\partial \lambda_1} \quad (\text{A.7a})$$

$$T_2 = \frac{1}{\lambda_1} \frac{\partial W}{\partial \lambda_2} \quad (\text{A.7b})$$

4 Eqs. (A.5)–(A.8) are the system of equations governing the unknowns T_1 , T_2 , K_1 , K_2 , λ_1 , λ_2 , ξ , and ρ .

5 At this point, it is helpful to rearrange Eq. (A. 6a) into a more suitable form for numerical calculation. Since T_1 is a
 6 function of λ_1 and λ_2 , $\frac{dT_1}{d\rho}$ can be defined as

$$\frac{dT_1}{d\rho} = \frac{\partial T_1}{\partial \lambda_1} \frac{\partial \lambda_1}{\partial r} \frac{\partial r}{\partial \rho} + \frac{\partial T_1}{\partial \lambda_2} \frac{\partial \lambda_2}{\partial r} \frac{\partial r}{\partial \rho} \quad (\text{A.8})$$

7 Differentiating Eq. (A.4b) gives

$$\frac{d\lambda_2}{dr} = \frac{(\rho' - \lambda_2)}{r} \quad (\text{A.9})$$

8 Substituting for $\frac{dT_1}{d\rho}$ from Eq. (A. 9) into Eq. (A.6a), and rearranging in terms of $\frac{d\lambda_1}{dr}$ gives

$$\frac{d\lambda_1}{dr} = \frac{\partial T_2}{\partial \lambda_1}^{-1} \left(-\frac{(\rho' - \lambda_2)}{r} \left(\frac{\partial T_1}{\partial \lambda_2} \right) - \frac{\rho'(T_2 - T_1)}{r\lambda_2} \right) \quad (\text{A.10})$$

9 The final equation is obtained by substituting for K_1 and K_2 in Eq. (A.4b). The expression for K_1 and K_2 are taken
 10 from Eq. (A.6) in terms of ρ^{η}

$$\rho'' = \frac{d\rho'}{dr} = \frac{\rho' d\lambda_2}{\lambda_1 dr} + \left(\frac{\lambda_1^2 - \rho'^2}{r\lambda_2} \right) \left(\frac{T_2}{T_1} \right) \quad (\text{A.11})$$

- 1 The right-hand side of Eqs. (A.10) - (A.12) are all functions of λ_1 , λ_2 , ρ , r . In the contact region, the membrane
2 deforms to the surface of the spherical indenter, so that

$$\rho = R \left(\sin \frac{\xi}{R} \right) \quad (\text{A.12})$$

- 3 With this relation, the number of equations can be reduced by one.

$$\rho' = \lambda_1 \left(\cos \frac{\xi}{R} \right) \quad (\text{A.13a})$$

$$\lambda_2 = \frac{\sin \frac{\xi}{R}}{r} \quad (\text{A.13b})$$

- 4 The governing equation of deformation for the contact region are defined when Eqs. (A.13) and (A.14) are
5 substituted into Eqs. (A.9) - (A.11).

- 6 The direct experimental measurements of importance to this study are the vertical load applied to the spherical
7 indenter and the deflection at the centre of the membrane, $r=0$, due to the applied vertical load. The vertical load, f ,
8 can be obtained from $T_1(a)$ as

$$f = h2\pi\rho(a)T_1(a) \left[1 - \frac{\rho'^2}{\lambda_1^2} \right]^{\frac{1}{2}} \quad (\text{A.14a})$$

- 9 The deflection at the centre of the membrane is the total distance of indentation, d , and is defined as

$$d = \int_0^{r_c} [\lambda_1^2(r) - \rho'^2(r)]^{\frac{1}{2}} dr + \int_{r_c}^a [\lambda_1^2(r) - \rho'^2(r)]^{\frac{1}{2}} dr \quad (\text{A.14b})$$

- 10 Where the integrands take the values from the solutions of the corresponding regions.

- 11 The pole, at the center of the membrane defines a condition of symmetry so that

$$\xi(0) = 0 \quad (\text{A.15a})$$

1 and an assumption that

$$\lambda_1(0) = \lambda_0 \quad (\text{A.15b})$$

2 where λ_0 is a value of possible stretch ratio at the pole.

3 As the experimental indentation range is known prior to solving for the material coefficients C_{10} and C_{01} , a set of λ_0
 4 is assumed that approximates the range of experimental indentations measured. Once λ_0 is identified, the equations
 5 of deformation in the contact region can be integrated. A second assumption is made for the size of the contact
 6 region in terms of $\rho(r_c)$, where r_c is the contact radius. The integration procedure for the contact region is terminated
 7 when $r=r_c$. The end values of $\rho, \lambda_1, \lambda_2$ computed from the contact solution at r_c serve as the initial conditions for
 8 integration of the deformation equations in the noncontact region, which is terminated at $r=a$. The assumed values of
 9 λ_0 and r_c are correctly paired only if the calculated value of $\lambda_2(a)$ equals the value of pre-stretch ratio, λ_p . The value
 10 of $\lambda_2(a)$ remains constant during the deformation since the membrane is fixed at $\rho(a)$. If the condition is not satisfied,
 11 another r_c is assumed and the equations of deformation are reintegrated until $\lambda_2(a) = \lambda_p$, for all values of λ_0 . Once this
 12 condition is satisfied, the vertical load and indentation are identified for the range of λ_0 . These analytical force
 13 indentations are compared to the experimental data set. This procedure is continued until a set of C_{10} and C_{01}
 14 Mooney Rivlin coefficients are identified which characterise the analytical load-indentation set to be within a
 15 specified tolerance of the experimental load-indentation set. The material coefficients are also checked for stability
 16 through employing thermodynamic considerations by employing the positive work criteria, as described by Eq.
 17 (A.16), coupled with coefficient positivity.

$$W = W(I_1, I_2) \geq 0 \quad (\text{A.16})$$

18 The fourth order Runge-Kutta method is employed for all integrations carried out. All numerical calculations and
 19 minimisation routines were developed and solved with Matlab 7.8 (r2009a, Natick, Massachusetts: The MathWorks
 20 Inc., 2009).

REFERENCES

- [1] Badylak SF. The extracellular matrix as a biologic scaffold material. *Biomaterials* 2007;28:3587-93.
- [2] Badylak SF, Freytes DO, Gilbert TW. Extracellular matrix as a biological scaffold material: Structure and function. *Acta Biomaterialia* 2009;5:1-13.
- [3] Piterina A, Cloonan A, Meaney C, Davis L, Callanan A, Walsh M, et al. ECM-Based Materials in Cardiovascular Applications: Inherent Healing Potential and Augmentation of Native Regenerative Processes. *International Journal of Molecular Sciences* 2009;10:4375-417.
- [4] Robinson KA, Li JS, Mathison M, Redkar A, Cui JH, Chronos NAF, et al. Extracellular matrix scaffold for cardiac repair. *Circulation* 2005;112:1135-143.
- [5] Zantop T, Gilbert TW, Yoder MC, Badylak SF. Extracellular matrix scaffolds are repopulated by bone marrow-derived cells in a mouse model of achilles tendon reconstruction. *Journal of Orthopaedic Research* 2006;24:1299-309.
- [6] Badylak S, Kokini K, Tullius B, Whitson B. Strength over Time of a Resorbable Bioscaffold for Body Wall Repair in a Dog Model. *Journal of Surgical Research* 2001;99:282-7.
- [7] Tottey S, Johnson SA, Crapo PM, Reing JE, Zhang L, Jiang H, et al. The effect of source animal age upon extracellular matrix scaffold properties. *Biomaterials* 2011;32:128-36.
- [8] Raghavan D, Kropp BP, Lin H-K, Zhang Y, Cowan R, Madhally SV. Physical characteristics of small intestinal submucosa scaffolds are location-dependent. *Journal of Biomedical Materials Research Part A* 2005;73A:90-6.
- [9] Freytes DO, Stoner RM, Badylak SF. Uniaxial and biaxial properties of terminally sterilized porcine urinary bladder matrix scaffolds. *J Biomed Mater Res B Appl Biomater* 2008;84:408-14.
- [10] Humphrey JD. Computer Methods in Membrane Biomechanics. *Comput Methods Biomech Biomed Engin* 1998;1:171-210.
- [11] Billiar KL, Sacks MS. Biaxial Mechanical Properties of the Natural and Glutaraldehyde Treated Aortic Valve Cusp---Part I: Experimental Results. *Journal of Biomechanical Engineering* 2000;122:23-30.
- [12] Sacks M. Biaxial Mechanical Evaluation of Planar Biological Materials. *Journal of Elasticity* 2000;61:199-246.
- [13] Gilbert TW, Wognum S, Joyce EM, Freytes DO, Sacks MS, Badylak SF. Collagen fiber alignment and biaxial mechanical behavior of porcine urinary bladder derived extracellular matrix. *Biomaterials* 2008;29:4775-82.
- [14] Lally C, Reid AJ, Prendergast PJ. Elastic Behavior of Porcine Coronary Artery Tissue Under Uniaxial and Equibiaxial Tension. *Ann Biomed Eng* 2004;32:1355-64.
- [15] Vande Geest JP, Sacks MS, Vorp DA. The effects of aneurysm on the biaxial mechanical behavior of human abdominal aorta. *Journal of Biomechanics* 2006;39:1324-34.
- [16] Prendergast PJ, Lally C, Daly S, Reid AJ, Lee TC, Quinn D, et al. Analysis of Prolapse in Cardiovascular Stents: A Constitutive Equation for Vascular Tissue and Finite-Element Modelling. *Journal of Biomechanical Engineering* 2003;125:692-9.
- [17] Eilaghi A, Flanagan JG, Tertinegg I, Simmons CA, Wayne Brodland G, Ross Ethier C. Biaxial mechanical testing of human sclera. *Journal of Biomechanics* 2010;43:1696-701.
- [18] Waldman SD, Lee JM. Effect of sample geometry on the apparent biaxial mechanical behaviour of planar connective tissues. *Biomaterials* 2005;26:7504-13.
- [19] Waldman SD, Michael Lee J. Boundary conditions during biaxial testing of planar connective tissues. Part I: dynamic behavior. *J Mater Sci Mater Med* 2002;13:933-8.
- [20] Waldman SD, Sacks MS, Lee JM. Imposed state of deformation determines local collagen fibre orientation but not apparent mechanical properties. *Biomed Sci Instrum* 1999;35:51-6.
- [21] Reing JE, Brown BN, Daly KA, Freund JM, Gilbert TW, Hsiong SX, et al. The effects of processing methods upon mechanical and biologic properties of porcine dermal extracellular matrix scaffolds. *Biomaterials* 2010;31:8626-33.
- [22] Roth J, Dexter D, Lumpkins K, Bochicchio G. Hydrated vs. freeze-dried human acellular dermal matrix for hernia repair: a comparison in a rabbit model. *Hernia* 2009;13:201-7.
- [23] Wainwright JM, Czajka CA, Patel UB, Freytes DO, Tobita K, Gilbert TW, et al. Preparation of Cardiac Extracellular Matrix from an Intact Porcine Heart. *Tissue Engineering Part C: Methods* 2009;16:525-32.
- [24] Coburn JC, Brody S, Billiar KL, Pandit A. Biaxial mechanical evaluation of cholecyst-derived extracellular matrix: A weakly anisotropic potential tissue engineered biomaterial. *Journal of Biomedical Materials Research Part A* 2007;81A:250-6.
- [25] Whitson BA, Cheng BC, Kokini K, Badylak SF, Patel U, Morff R, et al. Multilaminate resorbable biomedical device under biaxial loading. *Journal of Biomedical Materials Research* 1998;43:277-81.
- [26] Freytes DO, Rundell AE, Vande Geest J, Vorp DA, Webster TJ, Badylak SF. Analytically derived material properties of multilaminated extracellular matrix devices using the ball-burst test. *Biomaterials* 2005;26:5518-31.
- [27] Floden EW, Malak SF, Basil-Jones MM, Negron L, Fisher JN, Lun S, et al. Biophysical characterization of ovine forestomach extracellular matrix biomaterials. *J Biomed Mater Res B Appl Biomater* 2010.
- [28] Horan R, Bramono D, Stanley J, Simmons Q, Chen J, Boepple H, et al. Biological and biomechanical assessment of a long-term bioresorbable silk-derived surgical mesh in an abdominal body wall defect model. *Hernia* 2009;13:189-99.
- [29] Ebenstein DM, Pruitt LA. Nanoindentation of biological materials. *Nano Today* 2006;1:26-33.
- [30] Yang WH, Feng WW. On axisymmetrical deformations of non-linear membranes. *Journal of Applied Mechanics* 1970;37:1002-11.
- [31] Yang WH, Hsu KH. Indentation of a Circular Membrane. *Journal of Applied Mechanics* 1971;38:227-9.

- 1 [32] Chou S-Y, Cheng C-M, LeDuc PR. Composite polymer systems with control of local substrate elasticity and their effect on
2 cytoskeletal and morphological characteristics of adherent cells. *Biomaterials* 2009;30:3136-42.
- 3 [33] Doyle BJ, Corbett TJ, Cloonan AJ, O'Donnell MR, Walsh MT, Vorp DA, et al. Experimental modelling of aortic aneurysms:
4 Novel applications of silicone rubbers. *Medical engineering & physics* 2009;31:1002-12.
- 5 [34] Doyle BJ, Cloonan AJ, Walsh MT, Vorp DA, McGloughlin TM. Identification of rupture locations in patient-specific
6 abdominal aortic aneurysms using experimental and computational techniques. *Journal of Biomechanics* 2010;43:1408-16.
- 7 [35] Freytes DO, Badylak SF, Webster TJ, Geddes LA, Rundell AE. Biaxial strength of multilaminated extracellular matrix
8 scaffolds. *Biomaterials* 2004;25:2353-61.
- 9 [36] Sobral JM, Caridade SG, Sousa RA, Mano JF, Reis RL. Three-dimensional plotted scaffolds with controlled pore size
10 gradients: Effect of scaffold geometry on mechanical performance and cell seeding efficiency. *Acta Biomater* 2011;7:1009-18.
- 11 [37] Selvadurai APS. Deflections of a rubber membrane. *Journal of the Mechanics and Physics of Solids* 2006;54:1093-119.
- 12 [38] Scott ON, Begley MR, Komaragiri U, Mackin TJ. Indentation of freestanding circular elastomer films using spherical
13 indenters. *Acta Materialia* 2004;52:4877-85.
- 14 [39] Record RD, Hillegonds D, Simmons C, Tullius R, Rickey FA, Elmore D, et al. In vivo degradation of 14C-labeled small
15 intestinal submucosa (SIS) when used for urinary bladder repair. *Biomaterials* 2001;22:2653-9.
- 16 [40] Boruch AV, Nieponice A, Qureshi IR, Gilbert TW, Badylak SF. Constructive Remodeling of Biologic Scaffolds is
17 Dependent on Early Exposure to Physiologic Bladder Filling in a Canine Partial Cystectomy Model. *Journal of Surgical Research*
18 2010;161:217-25.
- 19 [41] Hodde JP, Badylak SF, Shelbourne KD. The Effect of Range of Motion on Remodeling of Small Intestinal Submucosa (SIS)
20 When Used as an Achilles Tendon Repair Material in the Rabbit. *Tissue Engineering* 1997;3:27-37.
- 21 [42] Davis LM, Callanan A, Piterina AV, Doyle BJ, Walsh MT, McGloughlin TM. Storage Effects on the Mechanical and
22 Cellular Performance of Naturally Derived Extracellular Matrix Materials. In: Goh JCH, Lim CT, editors. 6th World Congress of
23 Biomechanics. Singapore: Springer Berlin Heidelberg; 2010. p. 139-42.
- 24 [43] Piterina AV, Meaney CL, Cloonan AJ, Davis LM, Walsh MT, McGloughlin TM. An Investigation of Ability of Novel
25 Vascular Graft Materials to Maintain a Contractile Phenotype of Smooth Muscle Cell under Flow Regimes within *In Vitro*
26 Bioreactors. BMES Annual Meeting. Pittsburgh, Pennsylvania, USA2009.
- 27 [44] Billiar K, Murray J, Laude D, Abraham G, Bachrach N. Effects of carbodiimide crosslinking conditions on the physical
28 properties of laminated intestinal submucosa. *J Biomed Mater Res* 2001;56:101-8.
- 29 [45] Dewey C, Straw B. Herd examination. In: Straw B, Zimmerman JJ, D'Allaire S, Taylor DJ, editors. *Diseases of Swine*. 9 ed.
30 Ames, Iowa: Blackwell Publishing; 2006. p. 3-13.
- 31 [46] Yoder JH, Elliott DM. Nonlinear and anisotropic tensile properties of graft materials used in soft tissue applications. *Clinical*
32 *Biomechanics* 2010;25:378-82.
- 33 [47] Derwin KA, Baker AR, Spragg RK, Leigh DR, Iannotti JP. Commercial Extracellular Matrix Scaffolds for Rotator Cuff
34 Tendon Repair. Biomechanical, Biochemical, and Cellular Properties. *J Bone Joint Surg Am* 2006;88:2665-72.
- 35 [48] Sacks MS, Gloeckner DC. Quantification of the fiber architecture and biaxial mechanical behavior of porcine intestinal
36 submucosa. *Journal of Biomedical Materials Research* 1999;46:1-10.
- 37 [49] Aron P, Alexander DC, Silvia W, Rebecca LH, Michael BC, Michael SS. Ex vivo deformations of the urinary bladder wall
38 during whole bladder filling: Contributions of extracellular matrix and smooth muscle. *Journal of Biomechanics* 2010;43:1708-
39 16.
- 40 [50] Sandor M, Xu H, Connor J, Lombardi J, Harper JR, Silverman RP, et al. Host response to implanted porcine-derived
41 biologic materials in a primate model of abdominal wall repair. *Tissue Eng Part A* 2008;14:2021-31.
- 42 [51] Alwitary A, Burns SJ, Abercrombie LC. Orbital implant exposure treatment with porcine dermal collagen patching. *Orbit*
43 2006;25:253-6.
- 44 [52] Kim KM, Herrera GA, Battarbee HD. Role of Glutaraldehyde in Calcification of Porcine Aortic Valve Fibroblasts. *Am J*
45 *Pathol* 1999;154:843-52.
- 46 [53] Giachelli CM. Ectopic Calcification : Gathering Hard Facts about Soft Tissue Mineralization. *Am J Pathol* 1999;154:671-5.
- 47 [54] Gandhi S, Kubba LM, Abramov Y, Botros SM, Goldberg RP, Victor TA, et al. Histopathologic changes of porcine dermis
48 xenografts for transvaginal suburethral slings. *Am J Obstet Gynecol* 2005;192:1643-8.
- 49 [55] Jarman-Smith ML, Bodamyali T, Stevens C, Howell JA, Horrocks M, Chaudhuri JB. Porcine collagen crosslinking,
50 degradation and its capability for fibroblast adhesion and proliferation. *J Mater Sci Mater Med* 2004;15:925-32.
- 51 [56] Ueno T, Pickett LC, de la Fuente SG, Lawson DC, Pappas TN. Clinical application of porcine small intestinal submucosa in
52 the management of infected or potentially contaminated abdominal defects. *J Gastrointest Surg* 2004;8:109-12.
- 53 [57] Abraham GA, Murray J, Bachrach NM. Bioengineered flat sheet graft prostheses In: Office USPaT, editor. A61F002/02 ed.
54 USA: Organogenesis, Inc. Canton MA; Mar 3, 2003.
- 55 [58] Konig G, McAllister TN, Dusserre N, Garrido SA, Iyican C, Marini A, et al. Mechanical properties of completely
56 autologous human tissue engineered blood vessels compared to human saphenous vein and mammary artery. *Biomaterials*
57 2009;30:1542-50.
- 58 [59] Gloeckner DC, Sacks MS, Billiar KL, Bachrach N. Mechanical evaluation and design of a multilayered collagenous repair
59 biomaterial. *J Biomed Mater Res* 2000;52:365-73.
- 60 [60] Davis NF, Mooney R, Callanan A, Flood HD, McGloughlin TM. Augmentation cystoplasty and extracellular matrix
61 scaffolds: an ex vivo comparative study with autogenous detubularised ileum. *PLoS One* 2011;6:e20323.
- 62 [61] Green AE, Adkins, J.E. . Large Elastic Deformations. London: Oxford University Press; 1970.

1 **Table Caption**

2 Table 1: Measured membrane properties and resolved Mooney-Rivlin material coefficients. Primary roughness
3 parameters: Average profile roughness (Ra), root-mean-square roughness (Rq), mean peak to valley height (Rz),
4 maximum peak height (Rp) and maximum valley height (Rv) were recorded as an average of 20 line profiles of 4
5 stereopairs per specimen. For exact definitions see ISO 4287.

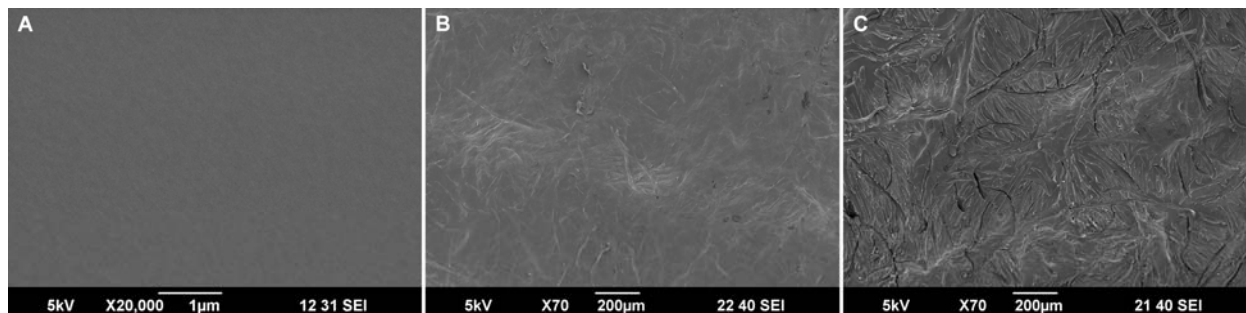
ACCEPTED MANUSCRIPT

1

Material	Thickness (μm)	Ball Burst Force (N)	C₁₀ (MPa)	C₀₁ (MPa)	Ra (μm)	Rq (μm)	Rz (μm)	Rp (μm)	Rv (μm)
PDMS	133 \pm 0.01	39.26 \pm 6.75	0.0393	0.47	0.02	0.03	0.16	0.17	0.17
UBM (2 ply)	209 \pm 19	85.96 \pm 29.41	9.3804	12.0488	4.32	5.56	23.21	23.82	14.78
UBM (4 ply)	280 \pm 12	168.2 \pm 12.24	7.4431	5.8335	6.70	8.78	32.27	32.99	21.90
SIS (2 ply)	185 \pm 16	73.67 \pm 7.66	8.9142	2.3225	8.94	12.71	39.20	23.93	56.48
SIS (4 ply)	205 \pm 21	133.53 \pm 21.31	7.4317	2.9508	9.69	14.24	53.21	29.00	70.96

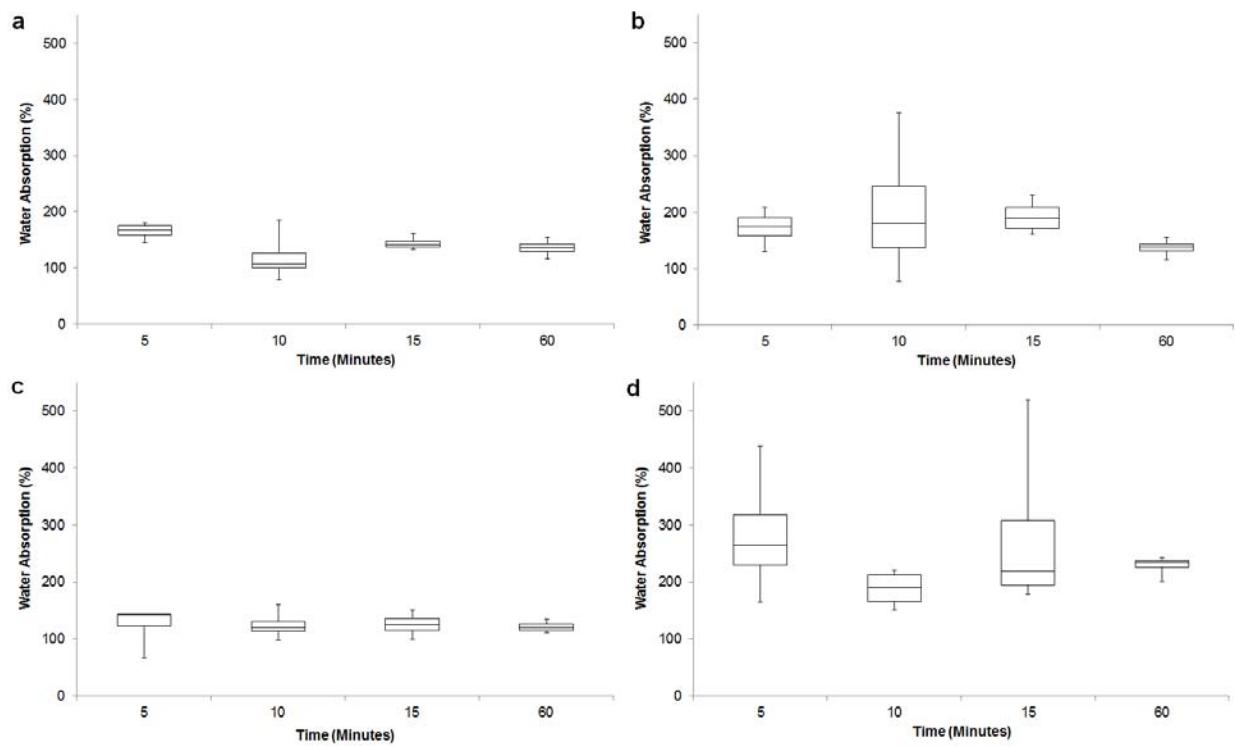
2

ACCEPTED MANUSCRIPT



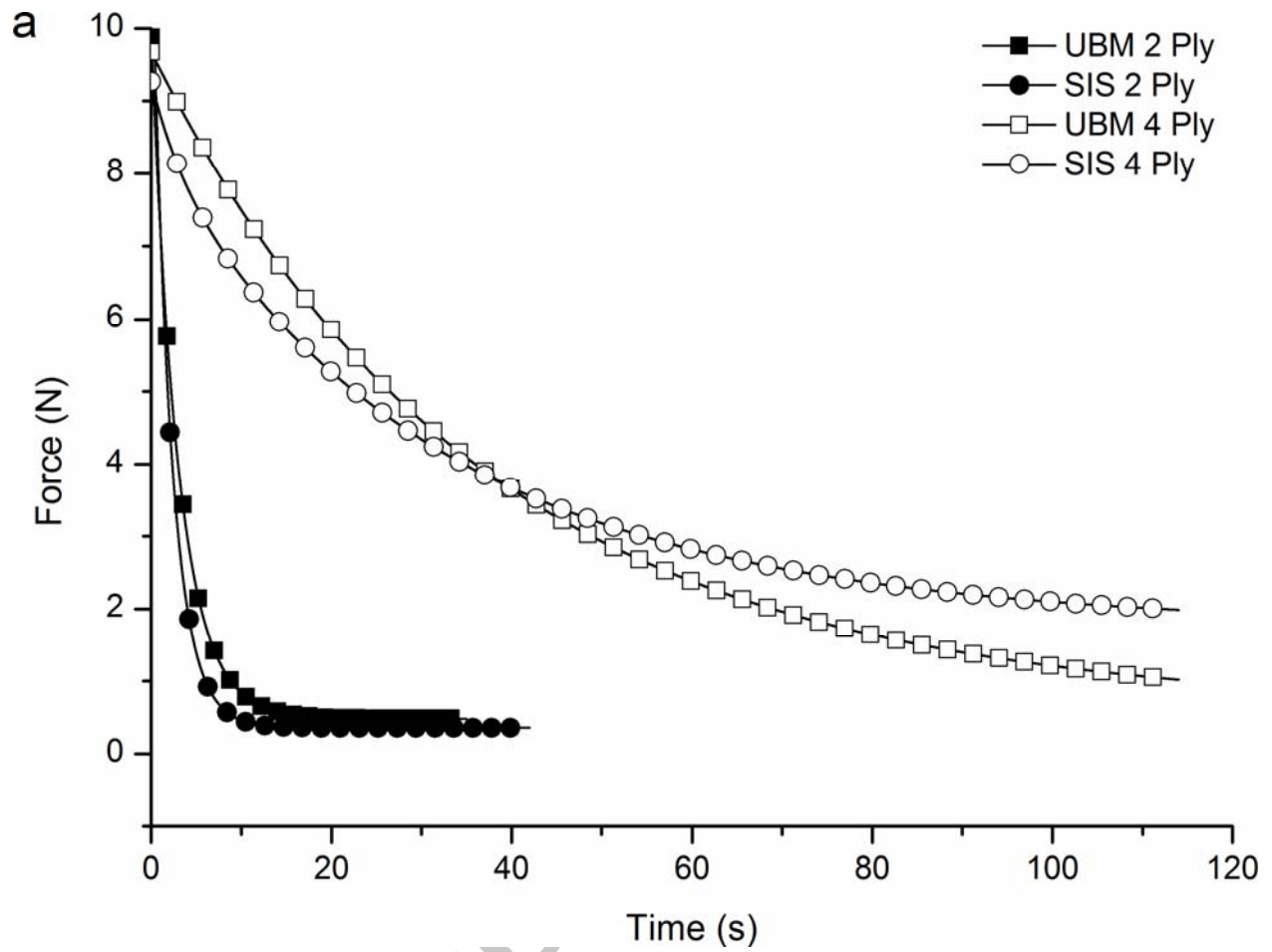
1

ACCEPTED MANUSCRIPT



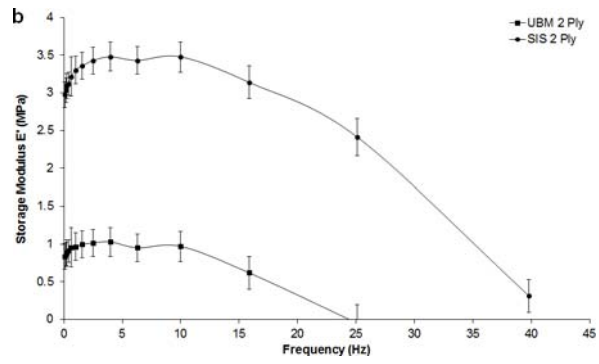
1

ACCEPTED MANUSCRIPT



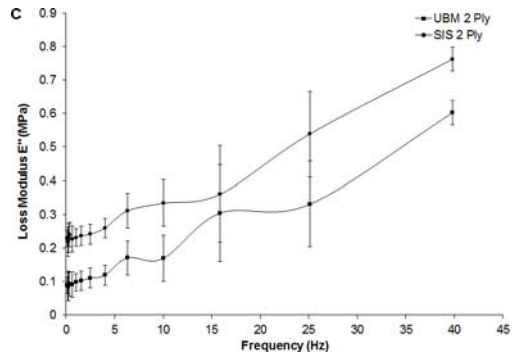
1

ACCEPTED



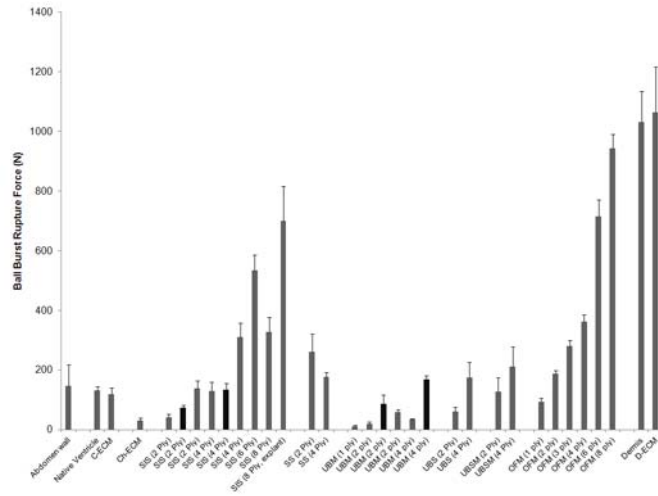
1

ACCEPTED MANUSCRIPT



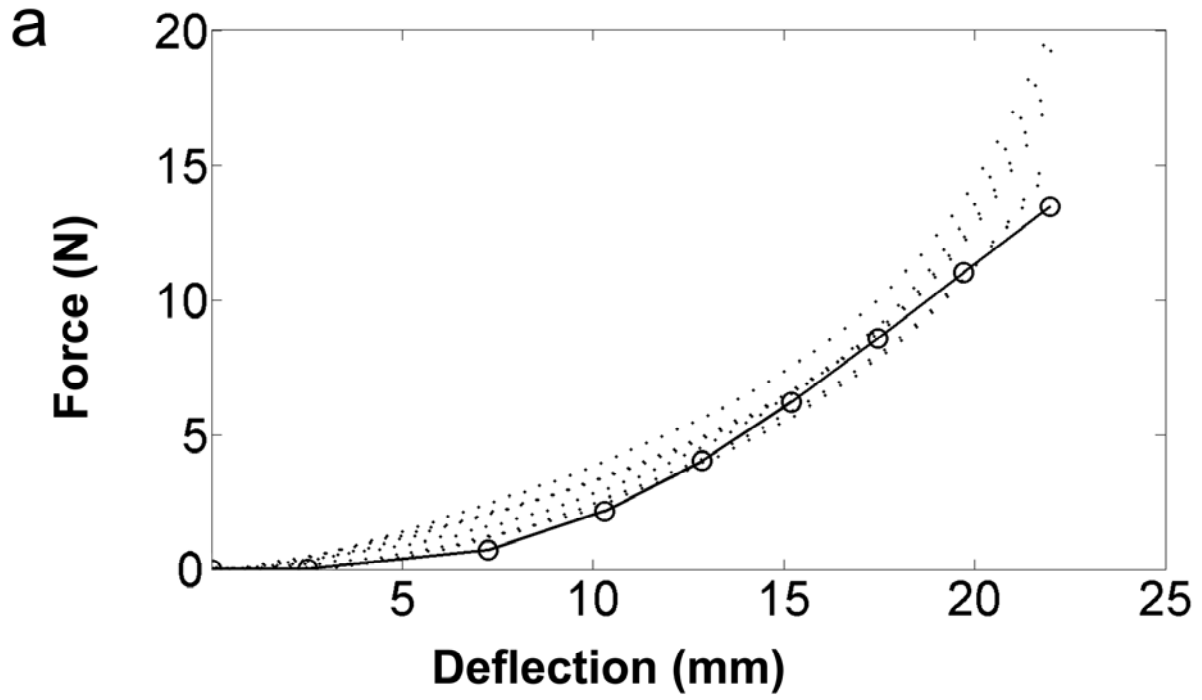
1

ACCEPTED MANUSCRIPT



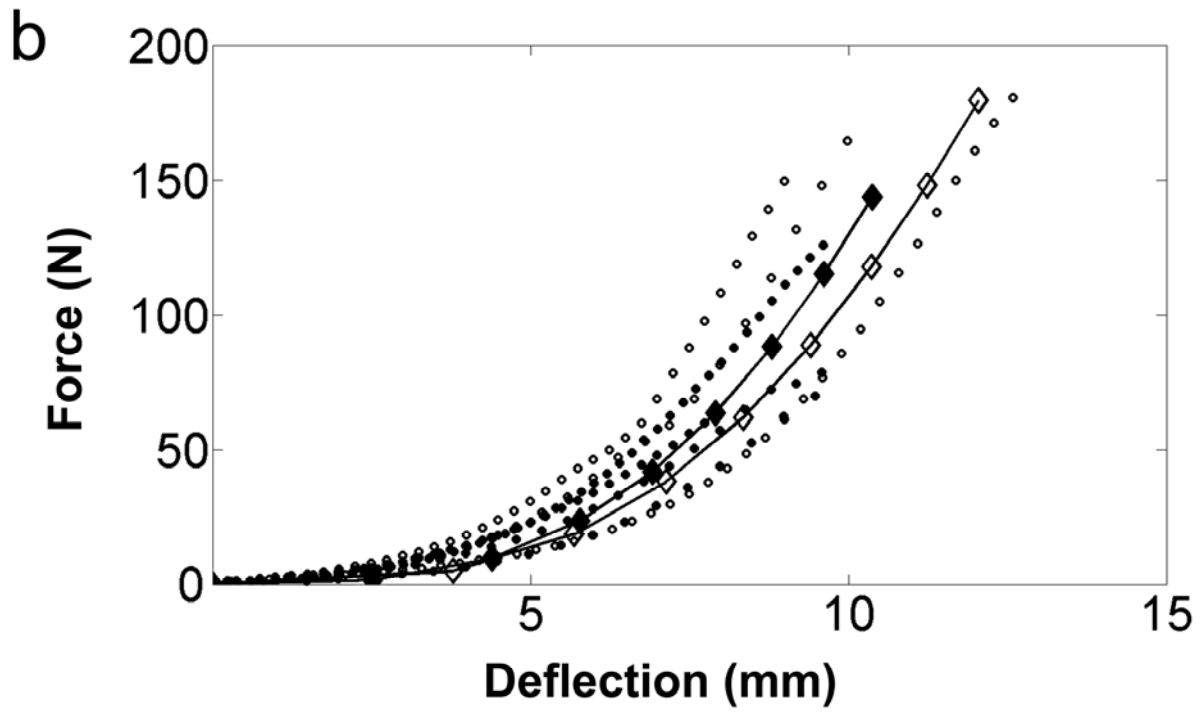
1

ACCEPTED MANUSCRIPT



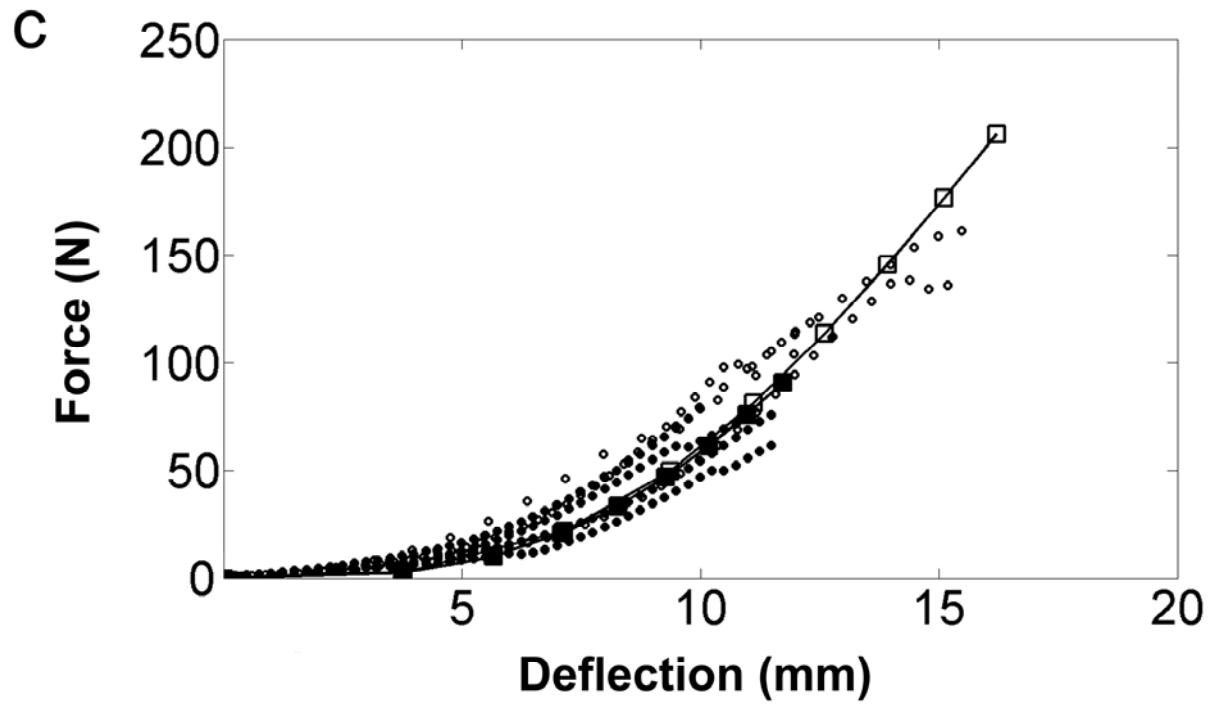
1

ACCEPTED MANUSCRIPT



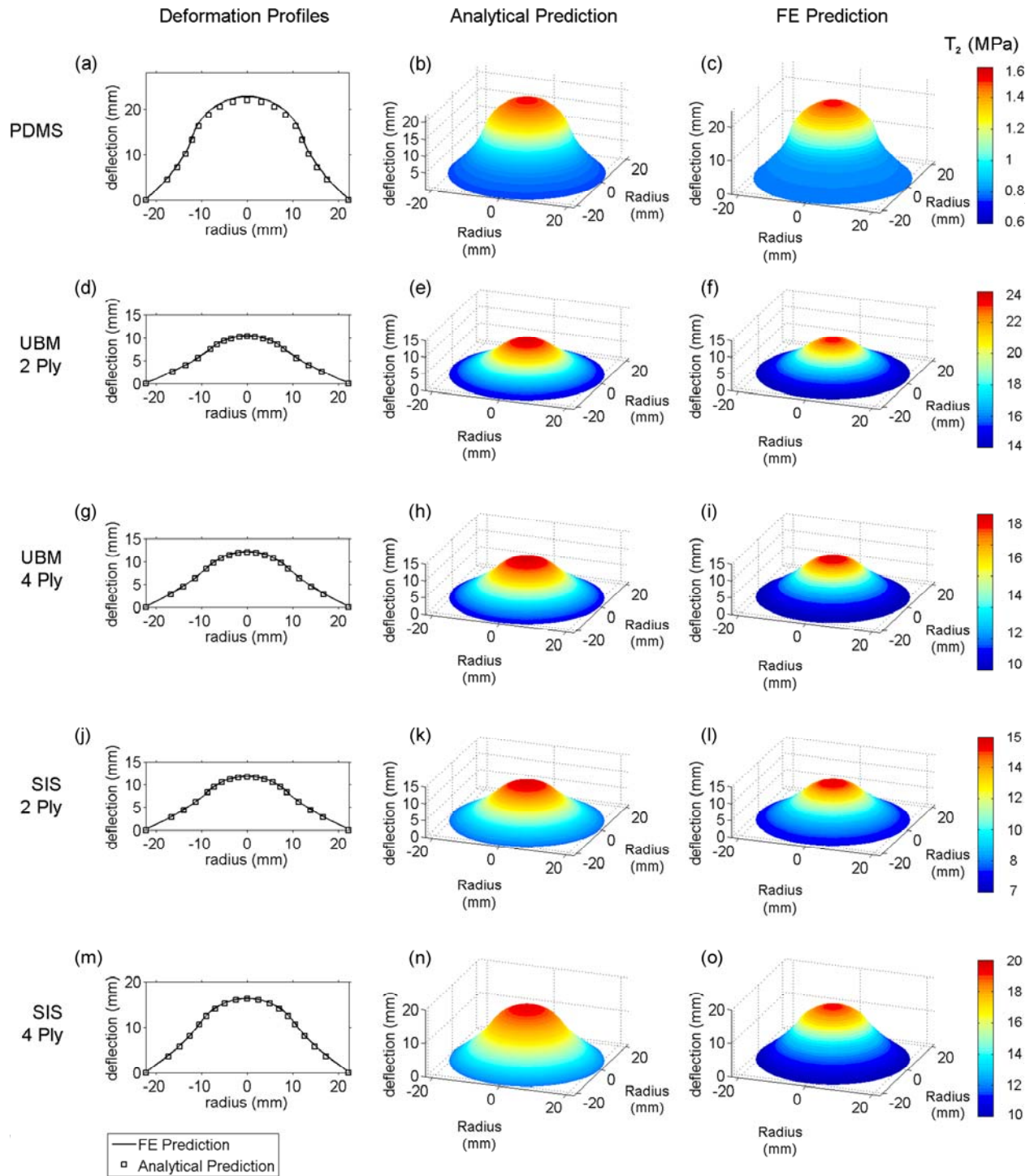
1

ACCEPTED MANUSCRIPT

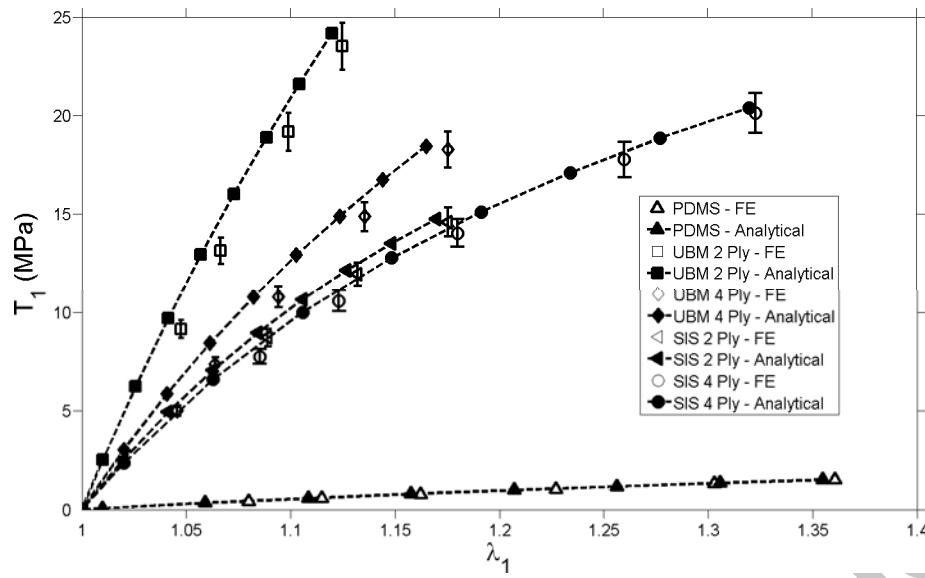


1

ACCEPTED MANUSCRIPT

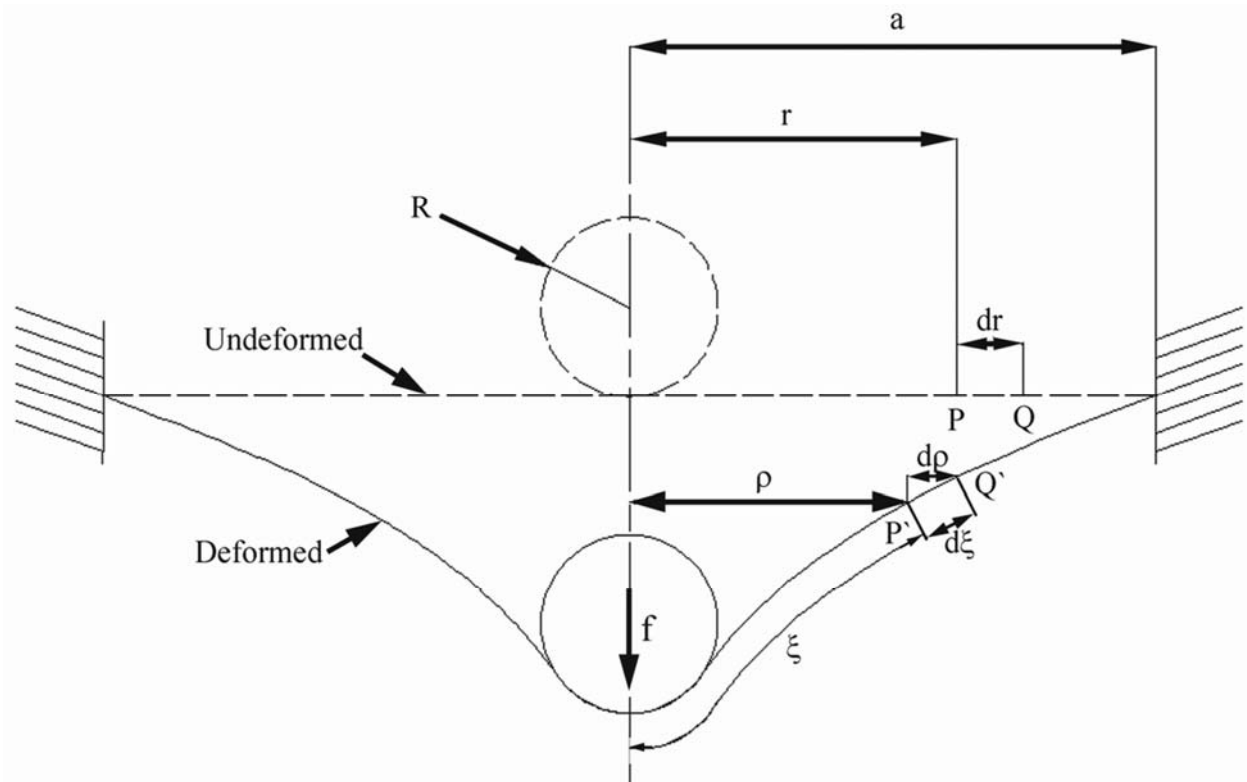


1



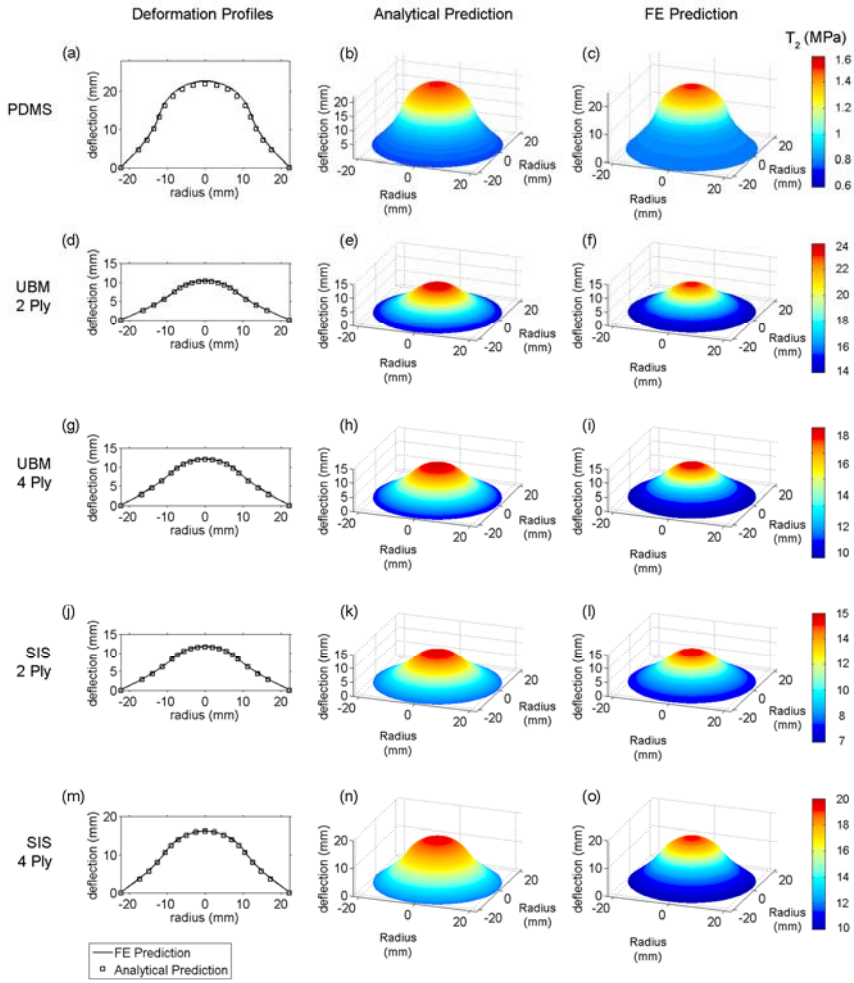
1

ACCEPTED MANUSCRIPT



1

ACCEPTED MANUSCRIPT



1

1 **Graphical Abstract Caption**

- 2 Indented free-standing membrane deformation profiles and the resolved analytical and finite element radial stress
3 contours on the outer membrane surface for (a-c) Poly(dimethylsiloxane) (PDMS), (d-i) Multilaminated Urinary
4 Bladder Matrix (UBM) and (j-o) Multilaminated Small Intestinal Submucosa (SIS).

ACCEPTED MANUSCRIPT

1 **Figure Captions**

2 Fig. 1. Representative SEM images of membrane materials (a) Poly(dimethylsiloxane) (PDMS), (b) Urinary Bladder
3 Matrix (UBM) and (c) Small Intestinal Submucosa (SIS).

4 Fig. 2. Box and whisker plots showing percentage water absorption of (a) 2 ply UBM, (b) 2 Ply SIS, (c) 4 Ply UBM,
5 (d) 4 ply SIS. The boxes indicate the 25th and 75th percentiles of the group intersected by the median line and the
6 whiskers display the maximum and minimum measurements.

7 Fig. 3. Effects of rehydration on ECM mechanical properties (a) hydration relaxation testing (b) E' response to
8 frequency and (c) E'' response to frequency.

9 Fig. 4. Ball burst rupture forces for the ECM materials evaluated in the current study (indicated in dark grey) and
10 previously published data for abdomen wall [6], dermis [21,22], ventricle [23], cardiac-ECM (C-ECM) [23],
11 cholecyst (Ch-ECM) [24], small intestinal submucosa (SIS) [6,25], urinary bladder matrix (UBM) [25,26], stomach
12 submucosa (SS) [26], urinary tunica propria and submucosa (UBS) [26], a combination UBM / UBS material termed
13 'UBSM' [26] and ovine forestomach matrix (OFM) [27]. Note the significant strength increase of explanted 8 ply
14 SIS after 2 years *in vivo*. Data represents mean burst force \pm standard deviation.

15 Fig. 5. Analytical model fitting based on experimental force-indentation data for (a) PDMS (\ominus), (b) 2 Ply (\blacklozenge) and
16 4 Ply (\blacklozenge) UBM, (c) 2 Ply (\blacksquare) and 4 Ply (\blacksquare) SIS. Closed and open circles represent 2 Ply and 4 Ply discrete data
17 points, respectively.

18 Fig. 6. Deformation profiles and the resolved analytical and finite element radial stress (T_2) contours on the outer
19 membrane surface for (a-c) PDMS, (d-f) 2 ply UBM, (g-i) 4 ply UBM, (j-l) 2 ply SIS and (m-o) 4 ply SIS.

20 Fig. 7. Circumferential stress resultant – stretch behavior resolved through analytical and numerical models. Error
21 bars indicate standard error.

22 Fig. A.1. Spherical indentation of a free-standing circular membrane based on the geometry deformation solution
23 originally proposed by Yang and Hsu in 1971 [31].

24 **All figures to be reproduced in colour on the Web and in black-and-white in print**
25

26

27

1

Nomenclature

Symbol	Description	Units	Symbol	Description	Units
a	Undeformed membrane radius	mm	r_c	Contact radius	mm
C_{10}, C_{01}	Mooney-Rivlin material constants	MPa	R	Indenter radius	mm
d	Displacement	mm	R_a	Average profile roughness	μm
E'	Storage modulus	MPa	R_q	Root-mean-square roughness	μm
E''	Loss modulus	MPa	R_z	Mean peak to valley height	μm
f	Force	N	R_p	Maximum peak height	μm
f	Frequency	Hz	R_v	Maximum valley height	μm
h	Thickness	μm	T_1, T_2	Circumferential, meridian stress resultant	N mm^{-1}
I_1, I_2	First, second deviatoric strain invariants	-	W	Strain energy potential	-
K_1	First principal curvature	-	λ	Stretch or stretch ratio	-
K_2	Second principal curvature	mm^{-1}	λ_p	Pre-stretch	-
\mathbf{P}'	Point on the deformed membrane	-	λ_0	Stretch range	-
PQ	Infinitesimal radial line	-	$\lambda_1, \lambda_2, \lambda_3$	Meridian, circumferential, transverse stretch	-
$\mathbf{P}'\mathbf{Q}'$	Meridian arc on the deformed surface	-	ρ	Horizontal distance from \mathbf{P}' to the axis of symmetry (deformed configuration)	mm
r	Plane polar coordinate	-	ξ	Meridian arc length (deformed configuration)	mm

2

3

4

Elsevier Editorial System(tm) for Acta Biomaterialia
Manuscript Draft

Manuscript Number: AB-11-545R1

Title: Spherical Indentation of free-standing acellular Extracellular Matrix membranes

Article Type: Full Length Article

Keywords: Soft tissue biomechanics; Decellularised tissue; Small Intestinal Submucosa; Urinary Bladder Matrix; Silicone elastomer; Membrane.

Corresponding Author: Mr Aidan J Cloonan, B.Sc.

Corresponding Author's Institution: University of Limerick

First Author: Aidan J Cloonan, B.Sc.

Order of Authors: Aidan J Cloonan, B.Sc.; Michael R O'Donnell, PhD; William T Lee, PhD; Michael T Walsh, PhD; Eamonn De Barra, PhD; Timothy M McGloughlin, PhD

Abstract: Numerous scaffold materials have been developed for tissue engineering and regenerative medicine applications to replace or repair damaged tissues and organs. Naturally occurring scaffold materials derived from acellular xenogeneic and autologous extracellular matrix (ECM) are currently in clinical use. These biological scaffold materials possess inherent variation in mechanical properties. Spherical indentation or ball burst testing, has been commonly used to evaluate ECM and harvested tissue due to its ease of use and simulation of physiological biaxial loading, but has been limited by complex material deformation profiles. An analytical methodology has been developed and applied to experimental load-deflection data of a model hyperelastic material and lyophilised ECM scaffolds. An optimum rehydration protocol was developed based on water absorption, hydration relaxation and Dynamic Mechanical Analysis. The analytical methodology was compared to finite element simulations of the tests and excellent correlation was seen between the computed biaxial stress resultants and geometry deformations. A minimum rehydration period of 5 minutes at 37 °C was sufficient for the evaluated multilaminated ECM materials. The proposed approach may be implemented for convenient comparative analysis of ECM materials and source tissues, process optimisation or during lot release testing.